Determination of Transverse Magnetic and Charge Densities from Experimental Form Factors

Siddharth Venkat[1,3], Gerald A. Miller[2]

[1] *Virginia Polytechnic Institute and State University, Blacksburg, VA 24061-0002*
[2] *University of Washington, Seattle, WA 98195-1560*

(Dated: August 20, 2010)

I. INTRODUCTION

Form factors for particles can be determined both theoretically and experimentally. These form factors can be used to compute charge and magnetization densities. A recent experiment using muon hydrogen suggests that the proton may have a radius 4% smaller than originally thought [1]. The results, which contradict both previous experiments and existing models, motivate our study of the relationship between form factors and charge densities.

II. PRELIMINARY THEORY

Intuitively, we expect particles to be localized. That is, we expect densities associated with the particle to be well approximated by functions that are zero outside some maximum radius. This assumption, called the finite radius approximation (FRA), will greatly simplify the relationship between form factors and their associated densities.

Let $\rho(b)$ be a two-dimensional density function (we will later take this to be charge or magnetization density) and let $F(Q^2)$ be the associated form factor. We assume that F and ρ have radial symmetry and that $\rho(b) = 0$ for $b \geq R$. Since ρ is the fourier transform of F, this means F is band-limited. We proceed in the spirit of the Kramer sampling theorem. ρ can be expanded as

$$\rho(b) = \sum_{n=1}^{\infty} c_n J_0(X_n \frac{b}{R}) \tag{1}$$

where X_n is the n-th zero of J_0 and c_n is given by the formula

$$c_n = \frac{2}{R^2 J_1(X_n)^2} \int_0^R b\rho(b) J_0(X_n \frac{b}{R})\, db. \tag{2}$$

Since F is the inverse transform of ρ, we can write

$$\begin{aligned} F(Q^2) &= 2\pi \int_0^\infty b\rho(b) J_0(\frac{bQ}{\hbar})\, db \\ &= 2\pi \int_0^R b\rho(b) J_0(\frac{bQ}{\hbar})\, db. \end{aligned} \tag{3}$$

Using this formula, we get

$$\begin{aligned} c_n &= \frac{2}{R^2 J_1(X_n)^2} \int_0^R b\rho(b) J_0(X_n \frac{b}{R})\, db \\ &= \frac{1}{2\pi} \frac{2}{R^2 J_1(X_n)^2} F((X_n \frac{\hbar}{R})^2). \end{aligned} \tag{4}$$

This yields the following expression for $\rho(b)$:

$$\rho(b) = \frac{1}{\pi R^2} \sum_{n=1}^{\infty} J_1(X_n)^{-2} F((X_n \frac{\hbar}{R})^2) J_0(X_n \frac{b}{R}). \tag{5}$$

We now perform some preliminary analysis of this new expression. For $x \gg 1$, we can approximate $J_0(x)$ by

$$J_0(x) \approx \sqrt{\frac{2}{\pi x}} \cos(x - \frac{\pi}{4})$$

so we can approximate X_n by $(n + \frac{3}{4})\pi$ [2]. Then

$$\begin{aligned} J_1(x) &= -J_0'(x) \\ &\approx \sqrt{\frac{2}{\pi x}} \sin(x - \frac{\pi}{4}) + \frac{1}{2x} \sqrt{\frac{2}{\pi x}} \cos(x - \frac{\pi}{4}) \\ &\approx \sqrt{\frac{2}{\pi x}} \sin(x - \frac{\pi}{4}) + \frac{1}{2x} J_0(x) \end{aligned}$$

so

$$\begin{aligned} J_1(X_n) &\approx \sqrt{\frac{2}{\pi X_n}} \sin(X_n - \frac{\pi}{4}) \\ &\approx \sqrt{\frac{2}{\pi^2 (n + \frac{3}{4})}} \sin((n + \frac{3}{4})\pi - \frac{\pi}{4}) \\ &= (-1)^n 2^{1/2} \pi^{-1} ((n + \frac{3}{4}))^{-1/2}. \end{aligned} \tag{6}$$

It follows that for large n, the terms in the series Eq. (5) for $\rho(b)$ are of the form:

$$\frac{\pi}{2R^2}(n+\frac{3}{4})F((X_n\frac{\hbar}{R})^2)J_0(X_n\frac{b}{R}).$$

So for the series to converge everywhere, namely at b=0, we need F to fall faster than $Q^{-2}$for large Q.

The function $\rho(b)$ can be approximated by using a finite number of terms in the series Eq. (5). Because $(X_n\frac{\hbar}{R})^2$ serves as the Q^2 in the argument of F, cutting off the series at N terms is equivalent to taking $F(Q^2)=0$ for $Q^2>(X_N\frac{\hbar}{R})^2$.

If the assumption that $\rho(b)=0$ for $b\geq R$ holds for a given value of R, then it also holds for larger values of R. We can see from Eq. (5) that increasing R increases the frequency with which $F(Q^2)$ is sampled and therefore decreases the range that is sampled. As a consequence, an increase in R demands an increase in the number of terms in the approximation for ρ.

A quick result following from the fact that ρ is the Fourier transform of F is that the mean-square-radius $\langle b^2\rangle$ is given by

$$\langle b^2\rangle = -4\hbar^2\left.\frac{dF}{dQ^2}\right|_{Q^2=0}.$$

In this paper, we will use $R=5\sqrt{|\langle b^2\rangle|}$ as a rule of thumb. Numerical studies of the form factors considered in this paper have shown that this value of R is sufficiently large and that perturbations to this value lead to the same density functions. We expect this estimate to be useful for charged particles, but in the case of neutral particles the charge distribution may change sign multiple times, giving cancellation that leads to a $|\langle b^2\rangle|$ too small for our approximation.

We will now derive an expression that allows us to analyze the effectiveness of FRA. Since $\rho(b)$ is the Fourier transform of F, we can substitute

$$\rho(b)=\frac{1}{2\pi\hbar^2}\int_0^\infty qF(q)J_0(\frac{qb}{\hbar})\,dq \tag{7}$$

into Eq. (2) to get

$$c_n=\frac{1}{\pi\hbar^2R^2J_1(X_n)^2}\int_0^R\int_0^\infty qbF(q)J_0(\frac{qb}{\hbar})J_0(X_n\frac{b}{R})\,dq\,db$$

Integration over b can be done using a standard identity to yield

$$c_n=\frac{X_n}{\pi\hbar^2R^2J_1(X_n)}\int_0^\infty\frac{qF(q^2)J_0(\frac{qR}{\hbar})}{(\frac{X_n}{R})^2-(\frac{q}{\hbar})^2}\,dq \tag{8}$$

We will compare this expression for c_n to that of Eq. (4) to determine how well FRA works.

III. EXAMPLES

To demonstrate our method and explore its limitations, we now analyze two models of the form factor. For the first model, let the form factor be given by

$$F(Q^2) = \frac{1}{1 + \frac{Q^2}{\Omega^2}}$$

where $\Omega = 1$ GeV. Then the associated charge density is:

$$\rho(b) = \frac{1}{2\pi\hbar^2} \int_0^\infty \frac{q}{1 + \frac{q^2}{\Omega^2}} J_0(\frac{qb}{\hbar})\, dq.$$

We can compare to ρ to the approximation

$$\rho(b) \approx \sum_{n=1}^{N} c_n J_0(X_n \frac{b}{R})$$

The exact ρ and approximations are plotted in Fig. 1.

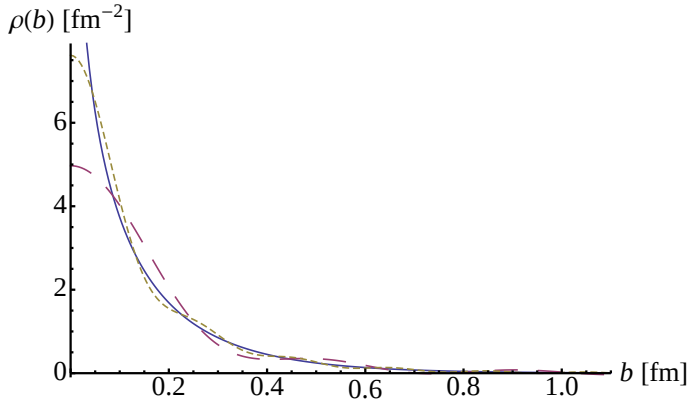

FIG. 1: Plot of ρ (solid), 10 term approximation (long dash) and 20 term approximation (short dash).

As we can see, our approximation is different from the exact result. The issue is that F falls as Q^{-2} for large Q and so the series does not converge everywhere. In particular, the exact form is singular at the origin, but a finite sum of terms cannot recover that behavior. However, away from the origin the series provides a working approximation of ρ. In order to determine the effectiveness of FRA, we compare the approximation coefficients Eq. (4) to those given by Eq. (8), which was derived from the orthogonality relation of J_0. A plot of the coefficients is given in Fig. 2. The graph shows that despite the singularity, the two expressions are almost identical

We now consider the dipole form factor given by

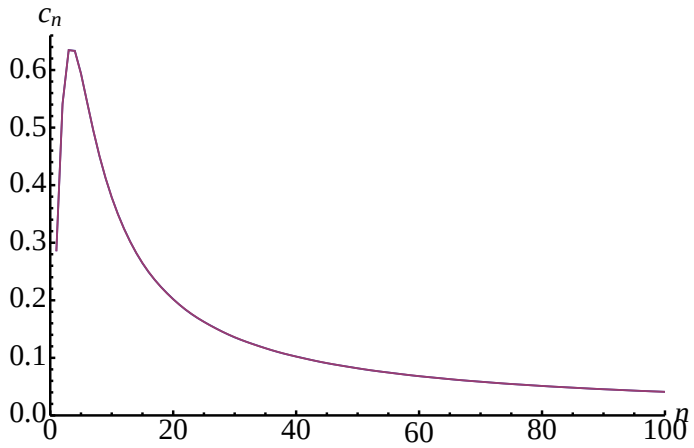

FIG. 2: Coefficients c_n for ρ derived using Eq. (4) and Eq. (8). The two expressions give the same values.

$$G_D(Q^2) = \frac{1}{(1+\frac{Q^2}{\Lambda^2})^2} \tag{9}$$

where $\Lambda = 0.71$ GeV. The dipole charge density is

$$\rho_d(b) = \frac{1}{2\pi\hbar^2}\int_0^\infty \frac{q}{(1+\frac{q^2}{\Lambda^2})^2} J_0(\frac{qb}{\hbar})\, dq.$$

We plot ρ_d and its approximations below.

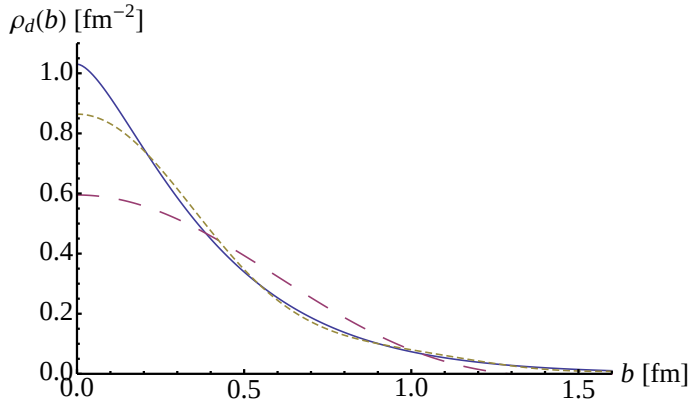

FIG. 3: Plot of ρ (solid), 5 term approximation (long dash) and 10 term approximation (short dash).

We can see how the approximations converge to the exact ρ_d. As before, we compare the coefficients given by Eq. (4) to those given by Eq. (8). They are plotted in Fig. 4

Again, the two expressions yield almost identical values. Since G_d falls faster than F, the coefficients fall faster as well. As a result, we need fewer terms to approximate ρ_d than we need for ρ.

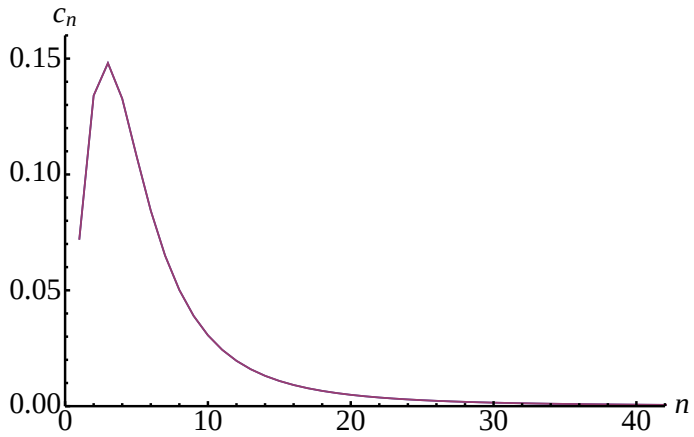

FIG. 4: Coefficients c_n for ρ_d derived using Eq. (4) and Eq. (8). The two expressions give the same values.

IV. RESULTS AND DISCUSSION

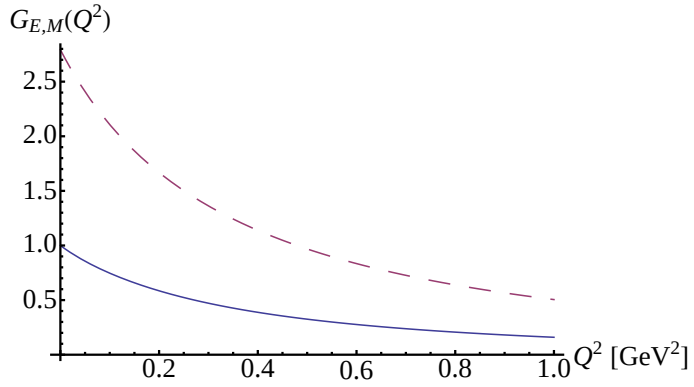

FIG. 5: The electromagnetic form factors $G_E(Q^2)$ (solid) and $G_M(Q^2)$ (dashed).

Light front theory allows us to recover the transverse charge density and ρ_{ch} as the two dimensional Fourier transform of F_1. Defining ρ_2 to be the two dimensional Fourier transform of F_2, we can obtain the magnetization density ρ_m using $\rho_m(b) = -b\frac{d}{db}\rho_2(b)$ [3]. F_1 and F_2 are given in terms of the form factors G_E and G_M by

$$F_1(Q^2) = \frac{G_E + \tau G_M}{1+\tau} \tag{10}$$

$$F_2(Q^2) = \frac{G_M - G_E}{1+\tau} \tag{11}$$

where

$$\tau(Q^2) = \frac{Q^2}{4M_p}. \tag{12}$$

The data for the proton form factors G_E and G_M have been fit to the forms

$$G_E(Q^2) = \frac{1 + \tau(p_6 + \tau(p_{10} + \tau p_{14}))}{1 + \tau(p_2 + \tau(p_4 + \tau(p_8 + \tau(p_{12} + \tau p_{16}))))} \tag{13}$$

$$G_M(Q^2) = \frac{1 + \tau\left(q_6 + \tau(q_{10} + \tau q_{14})\right)}{1 + \tau(q_2 + \tau(q_4 + \tau(q_8 + \tau\left(q_{12} + \tau q_{16}\right))))} \tag{14}$$

where the constants $p2, ..p16, q2, ..., q16$ are given in the following table [4].

i	p_i	q_i
2	1.104×10^1	3.517×10^1
4	1.385×10^1	3.530×10^1
6	-2.947×10^{-2}	2.318×10^1
8	2.430×10^1	1.958×10^3
10	7.347×10^{-1}	9.994×10^1
12	2.920×10^1	7.947×10^2
14	3.087×10^{-1}	-1.952×10^1
16	1.381×10^1	3.099×10^3

Substituting Eq. (12), Eq. (13) and Eq. (14) into Eq. (10) and Eq. (11), we get F_1 and F_2 as functions of Q^2, as plotted in Fig. 6.

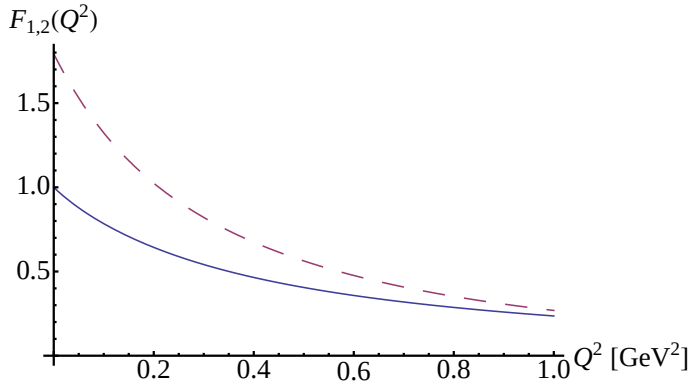

FIG. 6: The electromagnetic form factors $F_1(Q^2)$ (solid) and $F_2(Q^2)$ (dashed).

We now proceed according to FRA as outlined above. ρ_{ch} and ρ_2 can be approximated by:

$$\rho_{ch} = \frac{1}{\pi R_1^2} \sum_{n=1}^{N} J_1(X_n)^{-2} F_1((X_n \frac{\hbar}{R_1})^2) J_0(X_n \frac{b}{R_1}) \tag{15}$$

$$\rho_2 = \frac{1}{\pi R_2^2} \sum_{n=1}^{N} J_1(X_n)^{-2} F_2((X_n \frac{\hbar}{R_2})^2) J_0(X_n \frac{b}{R_2}). \tag{16}$$

Plots of these approximations are given in Fig. 7.

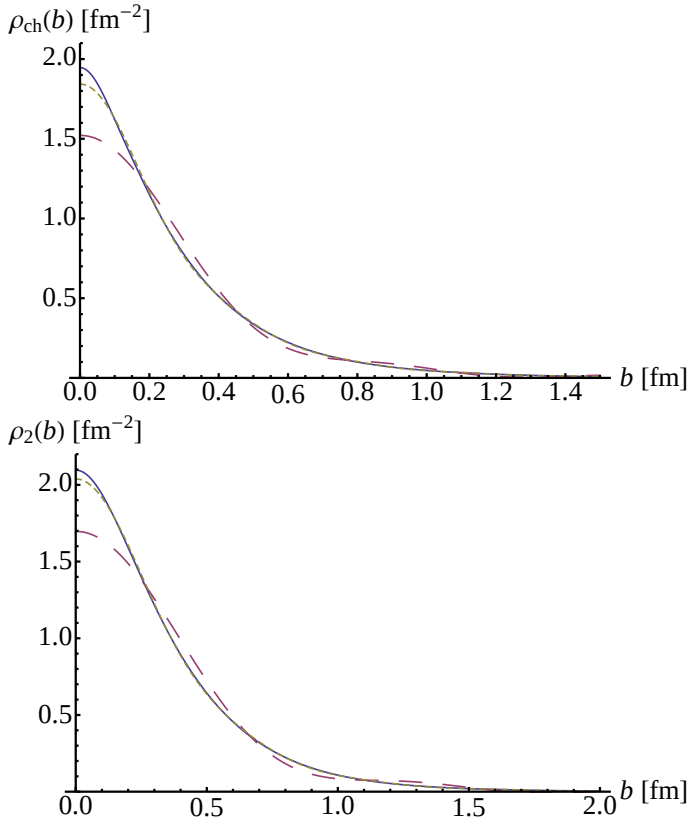

FIG. 7: Plots of approximations to ρ_{ch} and ρ_2 with 10 terms (long dash), 20 terms (short dash) and 50 terms (solid). The approximations converge as the number of terms increases.

As before, we compare the coefficients given by Eq. (4) to that given by Eq. (8). Plots of the coefficients are given in Fig. 8 and Fig. 9.

The errors in G_E and G_M were supplied by Arrington [4]. They are graphed in Fig. 10. We can derive the error in F_1 and F_2 by using Eq. (10) and Eq. (11):

$$(dF_1)^2 = (\frac{1}{1+\tau})^2 (dG_E)^2 + (\frac{\tau}{1+\tau})^2 (dG_M)^2 \tag{17}$$

$$(dF_2)^2 = (\frac{1}{1+\tau})^2 (dG_E)^2 + (\frac{1}{1+\tau})^2 (dG_M)^2 \tag{18}$$

We have assumed the errors in G_E, G_M are uncorrelated, and therefore add in quadrature. The data used to obtain the fits Eq. (13) and Eq. (14) have a maximum Q^2 of 30 GeV^2. By reasoning explained in [5], F_1 falls as Q^{-4} for large Q, so we extrapolate dF_1 for $Q^2 > 30$ GeV^2 by assuming dF_1 is continuous as $Q^2 = 30$ GeV^2 and that it also falls as Q^{-4}. Similary,

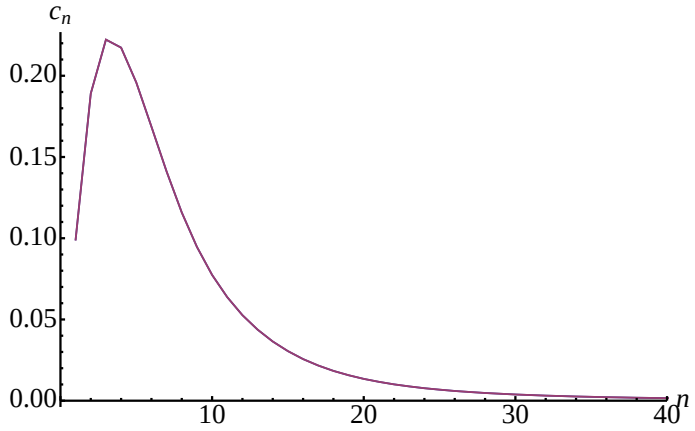

FIG. 8: Coefficients c_n for the electric charge density ρ_{ch} derived using Eq. (4) and Eq. (8). The two expressions give the same values.

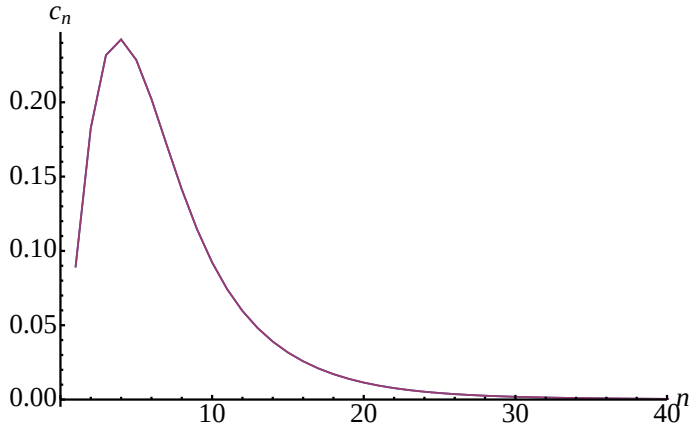

FIG. 9: Coefficients c_n for the magnetization density ρ_2 derived using Eq. (4) and Eq. (8). The two expressions give the same values.

experiment [6] and theory [7] suggest that F_2 falls as $\frac{F_1}{Q}$, so we extend dF_2 to the region with $Q^2 > 30$ GeV^2 by taking it to be continuous and assuming it falls as Q^{-5}. The functions dF_1 and dF_2 are plotted in Fig. 11. Eq. (15) and Eq. (16) allow us to derive an estimate for the error in ρ_{ch} and ρ_2 based on dF_1 and dF_2. Assuming the errors add constructively, we get

$$\begin{aligned} d\rho_{ch}(b) &= \sum_{n=1}^{\infty} \left| \frac{\partial \rho_{ch}(b)}{\partial F_1} \right| dF_1((X_n \frac{\hbar}{R_1})^2) \\ &= \frac{1}{\pi R_1^2} \sum_{n=1}^{\infty} |J_1(X_n)^{-2} J_0(X_n \frac{b}{R_1})| dF_1((X_n \frac{\hbar}{R_1})^2) \end{aligned} \tag{19}$$

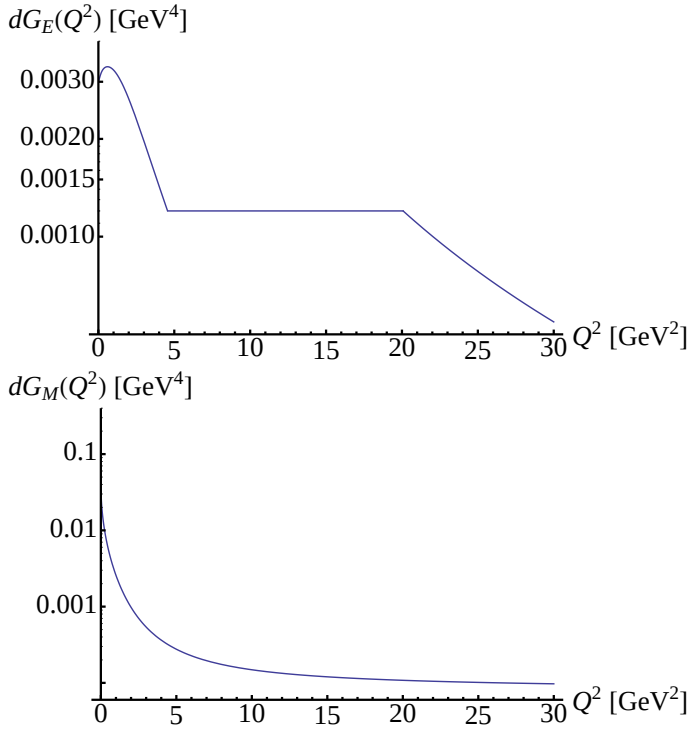

FIG. 10: Log plots of $dG_E(Q^2)$ and $dG_M(Q^2)$.

$$d\rho_2(b) = \sum_{n=1}^{\infty} \left| \frac{\partial \rho_2(b)}{\partial F_2} \right| dF_2((X_n \frac{\hbar}{R_2})^2)$$
$$= \frac{1}{\pi R_2^2} \sum_{n=1}^{\infty} |J_1(X_n)^{-2} J_0(X_n \frac{b}{R_2})| dF_2((X_n \frac{\hbar}{R_2})^2). \quad (20)$$

The first 50 terms of Eq. (19) and Eq. (20) are plotted in Fig. 13.

The functions F_1 and F_2 fall faster than Q^{-4} for large Q. The coefficients in the expansions Eq. (15) and Eq. (16) for ρ_{ch} and ρ_2 must fall faster than n^{-3} for large n by the analysis in section II. Thus, the coefficients for large n must be small (as demonstrated in Fig. 8 and Fig. 9). The sums from $n = 51$ to $n = 1000$ in the expansions for ρ_{ch} and ρ_2 are plotted in Fig. 12. These remainders are small compared to the 50 term approximations in Fig. 7. We are therefore justified in approximating ρ_{ch} and ρ_2 by the first 50 terms in their expansions. Similarly, since dF_1 falls as Q^{-4} and dF_2 falls even faster, $d\rho_{ch}$ and $d\rho_2$ can be approximated by the first 50 terms in their expansions. Again, the remainders from $n = 51$ to $n = 1000$ (plotted in Fig. 14) are small, so our approximation is valid.

Using $\rho_m(b) = -b\frac{d}{db}\rho_2(b)$, we get

$$\rho_m = \frac{1}{\pi R_1^2} \sum_{n=1}^{N} J_1(X_n)^{-2} \frac{X_n}{R_2} F_2((X_n \frac{\hbar}{R_1})^2) J_1(X_n \frac{b}{R_2}) \quad (21)$$

and by the same reasoning as before, the error formula

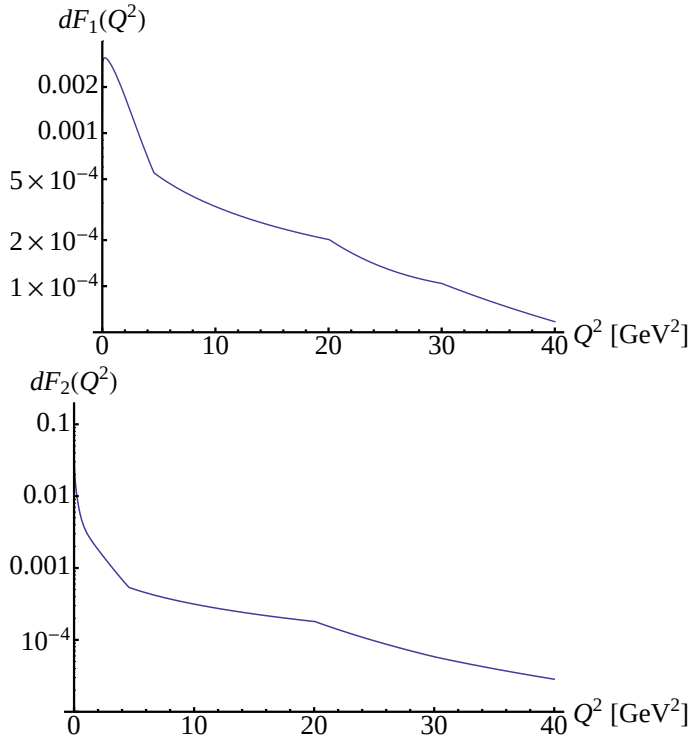

FIG. 11: Log plots of $dF_1(Q^2)$ and $dF_2(Q^2)$.

$$
\begin{aligned}
d\rho_m(b) &= \sum_{n=1}^{\infty} \left| \frac{\partial \rho_m(b)}{\partial F_2} \right| dF_2((X_n \frac{\hbar}{R_2})^2) \\
&= \frac{1}{\pi R_2^2} \sum_{n=1}^{\infty} |J_1(X_n)^{-2} \frac{X_n}{R_2} J_1(X_n \frac{b}{R_2})| dF_2((X_n \frac{\hbar}{R_2})^2). \qquad (22)
\end{aligned}
$$

We again approximate these two functions by the first first 50 terms of their respective series.

We now have working expressions for the charge density ρ_{ch}, the density ρ_2, the magnetization density ρ_m and their respective error functions $d\rho_{ch}$, $d\rho_2$ and $d\rho_m$. All three densities are plotted with their error bands in Fig. 15.

V. SUMMARY

We can see from Fig. 15 that the errors associated with the charge density is very small. This suggests that the transverse charge densities for the proton is almost completely determined. We can also see that near $b = 0$ the magnetization density is well known. The uncertainty is greater for larger b, but the magnetization density is constrained by the fact

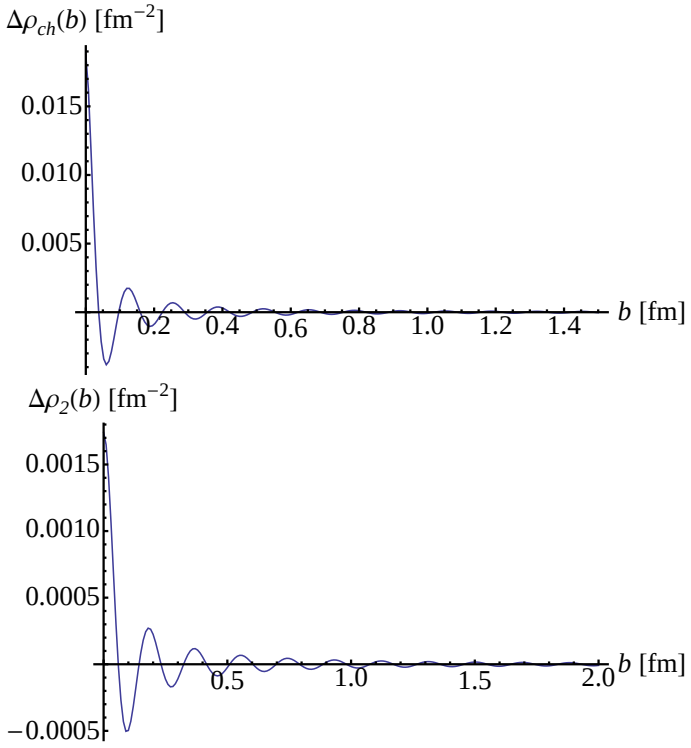

FIG. 12: Terms 51 to 1000 in Eq. (19) for ρ_{ch} and Eq. (20) for ρ_2.

that the total magnetization is fixed. Thus, we also have a reasonable idea for the magnetizatio density. However, this rests on the assumption that the form factors F_1 and F_2 are small for values of Q outside experimental range.

Acknowledgments

This research was supported by the NSF REU progam and US DOE. We thank Dr. Arrington for providing us with the fits for G_E, G_M and their uncertainties.

[1] R. Pohl *et al.*, Nature **466**, 213 (2010).
[2] J. D. Jackson, *Classical Electrodynamics Third Edition* (Wiley, New York, 1998)
[3] G. A. Miller, arXiv:1002.0355 [nucl-th].
[4] J. Arrington (private communication)
[5] J. J. Kelly, Phys. Rev. C **37**, 520 (1988).
[6] M. K. Jones *et al.* [Jefferson Lab Hall A Collaboration], Phys. Rev. Lett. **84**, 1398 (2000) [arXiv:nucl-ex/9910005].
[7] G. A. Miller and M. R. Frank, Phys. Rev. C **65**, 065205 (2002) [arXiv:nucl-th/0201021].

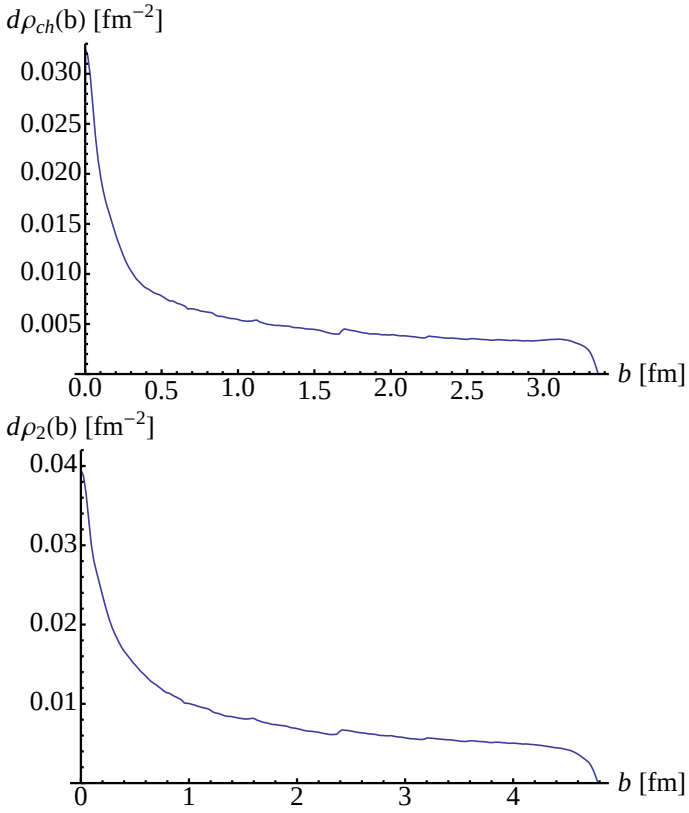

FIG. 13: The first 50 terms of $d\rho_{ch}$ and $d\rho_2$.

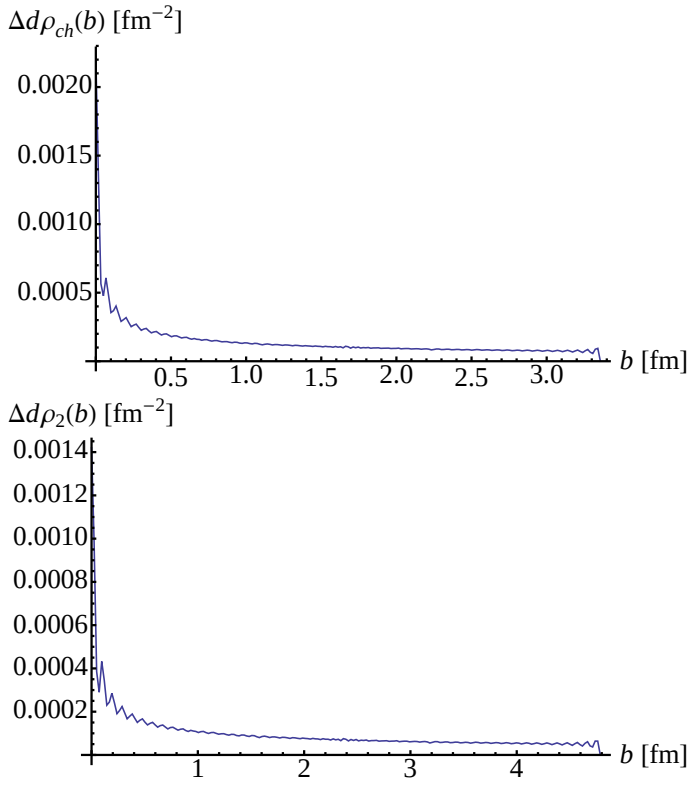

FIG. 14: Terms 51 to 1000 in Eq. (19) for $d\rho_{ch}$ and Eq. (20) for $d\rho_2$.

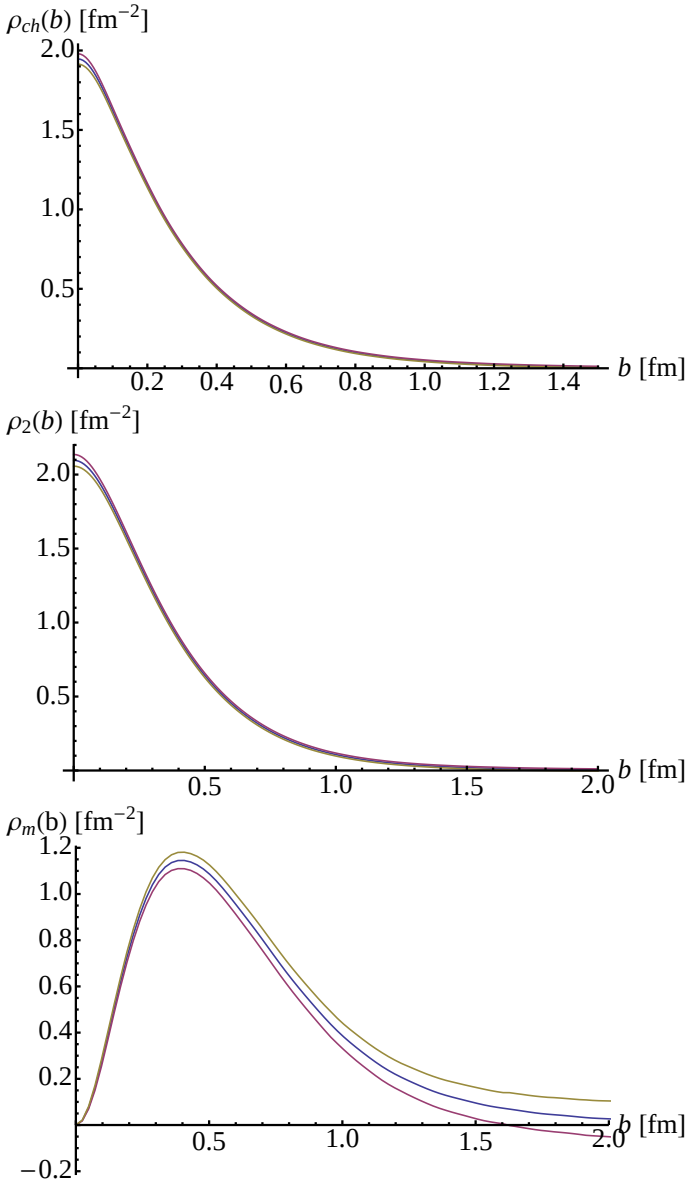

FIG. 15: The functions ρ_{ch}, ρ_2 and ρ_m with error bands $d\rho_{ch}$, $d\rho_2$ and $d\rho_m$, all approximated to 50 terms